Ferroelectric thin films with liquid crystal for gradient index applications

Oliver Willekens,[1,2,*] **John Puthenparampil George**,[1,2] **Kristiaan Neyts**,[1,2] **and Jeroen Beeckman**[1,2]

[1]*Liquid Crystals and Photonics group, ELIS Department, Ghent University, Sint-Pietersnieuwstraat 41, 9000 Ghent, Belgium*
[2]*Center for Nano- and Biophotonics (NB-Photonics), Ghent University, Belgium*
[*]*oliver.willekens@ugent.be*

Abstract: We report on the first ever combination of a thin film of lead zirconate titanate (PZT) with a liquid crystal (LC) layer. Many liquid crystal applications use a transparent conductive oxide to switch the liquid crystal. Our proposed processing does not, instead relying on the extremely high dielectric constant of the ferroelectric layer to extend the electric field from widely spaced electrodes over the liquid crystal. It eliminates almost entirely the fringe field problems that arise in nearly all the liquid crystal devices that use multiple addressing electrodes. We show, both via rigorous simulations as well as experiments, that the addition of a PZT layer over the addressing electrodes leads to a markedly improved LC switching performance at distances of up to 30 µm from the addressing electrodes with the current PZT-layer thickness of 0.84 µm. This improvement in switching is used to tune the focal length of the microlens with electrodes spaced at 30 µm.

OCIS codes: (230.3720) Liquid-crystal devices; (160.2260) Ferroelectrics; (110.2760) Gradient-index lenses.

References and links

1. H. Ren, Y.-H. Fan, S. Gauza, and S.-T. Wu, "Tunable-focus flat liquid crystal spherical lens," Appl. Phys. Lett. **84**, 4789–4791 (2004).
2. Y. Li and S.-T. Wu, "Polarization independent adaptive microlens with a blue-phase liquid crystal," Opt. Express **19**, 8045–8050 (2011).
3. S.-H. Lin, L.-S. Huang, C.-H. Lin, and C.-T. Kuo, "Polarization-independent and fast tunable microlens array based on blue phase liquid crystals," Opt. Express **22**, 925–930 (2014).
4. T. Nose and S. Sato, "A liquid crystal microlens obtained with a non-uniform electric field," Liq. Cryst. **5**, 1425–1433 (1989).
5. D. Resler, D. Hobbs, R. Sharp, L. Friedman, and T. Dorschner, "High-efficiency liquid-crystal optical phased-array beam steering," Opt. Lett. **21**, 689–691 (1996).
6. B. Apter, U. Efron, and E. Bahat-Treidel, "On the fringing-field effect in liquid-crystal beam-steering devices," Appl. Opt. **43**, 11–19 (2004).
7. P. F. McManamon, P. J. Bos, M. Escuti, J. Heikenfeld, S. Serati, H. Xie, and E. Watson, "A review of phased array steering for narrow-band electrooptical systems," Proc. IEEE **97**, 1078–1096 (2009).
8. S. R. Harris, "Polarization effects in nematic liquid crystal optical phased arrays," Proc. SPIE **5213**, 26–39 (2003).
9. L. Li, D. Bryant, T. V. Heugten, and P. J. Bos, "Near-diffraction-limited and low-haze electro-optical tunable liquid crystal lens with floating electrodes," Opt. Express **21**, 8371–8381 (2013).
10. L. Li, D. Bryant, and P. J. Bos, "Liquid crystal lens with concentric electrodes and inter-electrode resistors," Liq. Cryst. Rev. **2**, 130–154 (2014).
11. A. F. Naumov, M. Y. Loktev, I. R. Guralnik, and G. Vdovin, "Liquid-crystal adaptive lenses with modal control," Opt. Lett. **23**, 992–994 (1998).

#258864 Received 3 Feb 2016; revised 23 Mar 2016; accepted 27 Mar 2016; published 6 Apr 2016

12. Y. Li, Y. Liu, Q. Li, and S.-T. Wu, "Polarization independent blue-phase liquid crystal cylindrical lens with a resistive film," Appl. Opt. **51**, 2568–2572 (2012).
13. C.-T. Lee, Y. Li, H.-Y. Lin, and S.-T. Wu, "Design of polarization-insensitive multi-electrode grin lens with a blue-phase liquid crystal," Opt. Express **19**, 17402–17407 (2011).
14. J.-F. Blach, S. Saitzek, C. Legrand, L. Dupont, J.-F. Henninot, and M. Warenghem, "Batio3 ferroelectric nanoparticles dispersed in 5cb nematic liquid crystal: Synthesis and electro-optical characterization," J. Appl. Phys. **107**, 074102 (2010).
15. R. Shukla, C. Liebig, D. Evans, and W. Haase, "Electro-optical behaviour and dielectric dynamics of harvested ferroelectric linbo 3 nanoparticle-doped ferroelectric liquid crystal nanocolloids," RSC Adv. **4**, 18529–18536 (2014).
16. E. Mavrona, U. Chodorow, M. Barnes, J. Parka, N. Palka, S. Saitzek, J.-F. Blach, V. Apostolopoulos, and M. Kaczmarek, "Refractive indices and birefringence of hybrid liquid crystal-nanoparticles composite materials in the terahertz region," AIP Adv. **5**, 077143 (2015).
17. N. Izyumskaya, Y.-I. Alivov, S.-J. Cho, H. Morkoc, H. Lee, and Y.-S. Kang, "Processing, structure, properties, and applications of pzt thin films," Crit. Rev. Solid State Mater. Sci. **32**, 111–202 (2007).
18. J. P. George, P. F. Smet, J. Botterman, V. Bliznuk, W. Woestenborghs, D. Van Thourhout, K. Neyts, and J. Beeckman, "Lanthanide-assisted deposition of strongly electro-optic pzt thin films on silicon: Toward integrated active nanophotonic devices," ACS Appl. Mater. Interfaces **7**, 13350–13359 (2015). PMID: 26043103.
19. Q. Zou, H. E. Ruda, B. G. Yacobi, K. Saegusa, and M. Farrell, "Dielectric properties of lead zirconate titanate thin films deposited on metal foils," Appl. Phys. Lett. **77**, 1038–1040 (2000).
20. B. P. Zhu, D. D. Li, Q. F. Zhou, J. Shi, and K. K. Shung, "Piezoelectric pzt thick films on lanio 3 buffered stainless steel foils for flexible device applications," J. Phys. D: Appl. Phys. **42**, 025504 (2009).
21. R. Seveno and D. Averty, "Ultra light tunable capacitor based on pzt thin film deposited onto aluminium foil," J. Sol-Gel Sci. Technol. **68**, 175–179 (2013).
22. J. Walenza-Slabe and B. Gibbons, "Processing of rf-sputtered lead zirconate titanate thin films on copper foil substrates," J. Mater. Sci. **50**, 6420–6426 (2015).
23. P. J. Vanbrabant, J. Beeckman, K. Neyts, E. Willman, and F. A. Fernandez, "Diffraction and fringing field effects in small pixel liquid crystal devices with homeotropic alignment," J. Appl. Phys. **108**, 083104 (2010).
24. R. James, E. Willman, F. A. Fernández, and S. E. Day, "Finite-element modeling of liquid-crystal hydrodynamics with a variable degree of order," IEEE Trans. Electron Dev. **53**, 1575–1582 (2006).
25. D.-K. Yang and S.-T. Wu, "Tunable liquid crystal photonic devices," in *Fundamentals of Liquid Crystal Devices* (John Wiley & Sons, Ltd, 2006), pp. 347–374.

1. Introduction

Liquid crystals (LCs) are a unique class of materials, exhibiting properties of both liquids and solids. In particular, their unique electro-optic properties have been used in beam-steering devices, such as tunable angle deflectors and tunable lenses. The working principle is simple: by imposing a spatially varying optical path length (OPL)-profile over the area of an LC, one can change the propagation direction of light. Such a laterally varying OPL-profile is obtained by applying a non-uniform electric field over a liquid crystal. Inhomogeneous fields can be obtained with lenticulars [1–3] and hole-patterned arrays [4], which typically require only two electrodes, but also with multi-electrode designs. The latter category allows for a more accurate control of the phase front and can e.g. reduce spherical aberrations in liquid-crystal-based lenses, at the cost of having a more complex driving scheme. Multi-electrode designs typically consist of a large area common electrode on one substrate and a series of addressing electrodes on the other substrate. When the potential difference between neighboring addressing electrodes is small compared to the potential difference with the common electrode, a smooth transition of the orientation of the liquid crystal over the electrodes is usually obtained due to the viscoelastic interactions in the LC, provided the electrodes are sufficiently closely spaced [5]. However, in the region between two electrodes with a large potential difference, the effect of fringe fields can be pronounced [6]. This leads to a non-ideal distribution of the director, which is the vector representing the local volume average of the orientation of the liquid crystal molecules. This non-ideal orientation leads to undesired polarization changes, as well as a reduced beam-steering efficiency, because part of the light is directed elsewhere [6–8].

To reduce the complexity of a system having many closely spaced electrodes that need to be

#258864 Received 3 Feb 2016; revised 23 Mar 2016; accepted 27 Mar 2016; published 6 Apr 2016

addressed individually, several researchers have proposed configurations with a limited set of electrodes that are spaced further apart. A smooth variation of the potential difference over the liquid crystal can still be obtained by using floating electrodes [9] or a highly resistive layer connecting the addressing electrodes [10–12]. The resistive layer acts as a potential divider and causes a monotonic variation of the electric potential between neighboring electrodes. However, devices based on a resistive potential divider draw considerable current. In this paper, we demonstrate an alternative technique for realizing a gradual voltage drop, by using a layer with a high dielectric constant, ε. Although it is known that materials with high permittivity can be used as an alternative to resistive layers [13], to the best of our knowledge, this is the first report on the successful integration of liquid crystals with a ferroelectric thin film. Using the high permittivity of the ferroelectric thin film we demonstrate that a gradually varying potential between widely spaced electrodes can be obtained. The combination of ferroelectric solid state materials in the form of nanoparticles with liquid crystals has been an active research field in the past few years. Inclusion of the nanoparticles led to drastic improvement of switching voltage [14], the electro-optic response [15] or the optical properties in the THz region [16]. We expect that the combination of ferroelectric thin films with liquid crystal layers will lead to a similar improvement in certain liquid crystal switching modes.

2. Liquid crystal lens with ferroelectric layer

2.1. Characteristics of the deposited ferroelectric layer

The deposition of high-quality lead zirconate titanate (PZT) films on mono-crystalline substrates such as magnesium oxide or metallic layers such as platinum is well known [17]. Recently our group demonstrated that highly textured PZT thin films can be deposited on glass substrates using a cheap solution-based deposition method [18]. The process leads to a high-quality polycrystalline layer as shown in Fig. 1(a). The deposition of PZT on a glass substrate is a useful technique for e.g. piezoelectric sensors and actuators such as Microelectromechanical Systems (MEMS) and piezo touchscreens with tactile feedback, as well as for liquid crystal devices compatible with large active areas.

The relative dielectric constant ε_r of the PZT layer was characterized by measuring the capacitance of a 1 µm thick PZT layer sandwiched between two parallel disc-shaped Indium Tin Oxide (ITO) electrodes, each 3.14 mm^2 in area. In this configuration, it resembles a parallel plate capacitor for which the capacitance is given by:

$$C = \varepsilon_0 \varepsilon_r \frac{A}{d} \tag{1}$$

where A and d are the area of the electrodes and the spacing between them respectively. Because of the finite conductivity of the ITO electrodes at high frequencies the RC effects start to play a role, which limits the measurement of ε_r to frequencies below about 10 kHz. This is evident from the graph in Fig. 1(b): starting from about 10 kHz the permittivity decreases rapidly. When repeating the measurement using electrodes made from platinum, we observe no variation in the dielectric constant, up to 2 MHz.

The relative dielectric constant of the deposited PZT layer is measured to be $\varepsilon_{r,\|} \approx 550$ with low dielectric loss at 1 kHz [Fig. 1(b)], a frequency commonly used for switching liquid crystal. The measured dielectric constant is comparable to that found in other studies where PZT was deposited on metal foils using sol-gel processing and rf-sputtering [19–22].

2.2. Liquid crystal lens geometry

A liquid-crystal-based beam-steering device which has a radially varying optical path length acts as a lens. We used this device to study the effects of the PZT layer. A schematic cross-

#258864 Received 3 Feb 2016; revised 23 Mar 2016; accepted 27 Mar 2016; published 6 Apr 2016

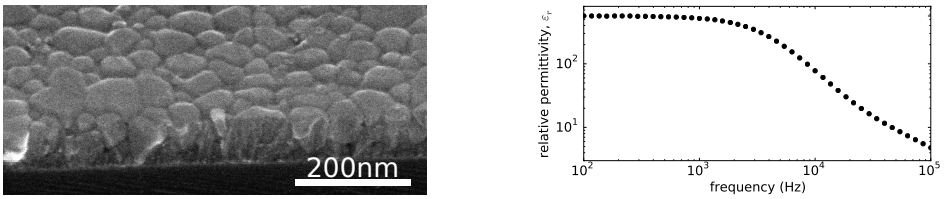

(a) (b)

Fig. 1. Characteristics of the PZT layer: (a) Scanning electron microscope image of a single PZT layer imaged from the side showing the polycrystalline nature of the deposited layer. Each single crystal grain has a diameter of ∼70 nm. (b) Measured relative dielectric constant of the PZT-layer, sandwiched between two ITO electrodes.

sectional view of the proposed PZT-enhanced liquid-crystal-based lens is shown in Fig. 2(a). From the bottom to the top, there is a glass substrate providing rigidity, on top of which ring-shaped concentric electrodes are deposited by means of standard lithographic processes. As the PZT layer is not influenced by the material of which the electrodes are made, we have made the electrodes of a non-transparent metal rather than the relatively costly ITO. This also allows us to study the microscope images more easily, at the expense of some unwanted diffraction. A small wedge in the rings is sacrificed to allow each ring to be connected to an externally applied voltage, by means of the addressing electrodes. A 10 nm thin buffer layer is deposited on the glass substrate and the electrodes to ensure good crystal growth of the PZT, which is the next layer in the stack and is about 0.84 µm thick. The minimally required thickness of this buffer layer was determined experimentally [18], while the thickness of the PZT layer was chosen as a compromise between processing time and the required amount of electric field averaging as predicted by the simulations. On top of the PZT layer is a thin polyimide (PI) alignment layer, which is in contact with the nematic liquid crystal. Another PI alignment layer, a single electrode spanning the entire width of the device and another glass substrate complete the stack.

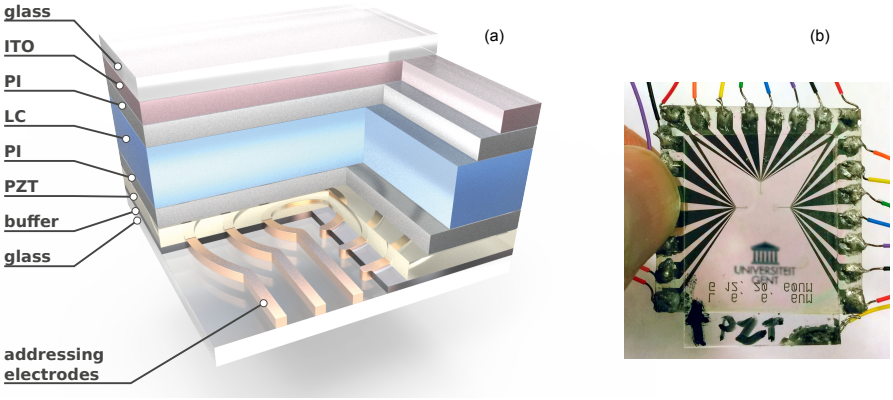

Fig. 2. (a) Schematic of the cross-sectional buildup of the liquid crystal lens with added PZT layer. Note that the thickness of each layer is not to scale. (b) A fabricated LC cell with PZT layer, containing 3 microlenses.

The full area electrode, which we will refer to as the common electrode, is transparent, as shown in Fig. 2(b), to allow the beam-steering device to be used in transmission, but it could be a non-transparent metal if reflective beam-steering was desired. The purpose of the alignment

#258864 Received 3 Feb 2016; revised 23 Mar 2016; accepted 27 Mar 2016; published 6 Apr 2016

layers is to impose a preferential direction to the nematic liquid crystal molecules. For these devices, we use the rubbing alignment technique to align the director parallel to the substrate and perpendicular to the straight sections of the addressing electrodes shown in Fig. 2(a).

3. Measurements and discussion

To evaluate the influence of PZT on the electric field distribution in the device, we fabricated a reference device without PZT, but otherwise identical to the test device. Both the reference device and the PZT-enhanced device are studied with a polarizing optical microscope, which allows to evaluate the birefringence as a function of position. The color that results from white light passing through a stack of crossed polarizers, with a uniaxial material in between and which has its c-axis at an angle different from 0° or 90° with respect to the transmission axis of either polarizer, is related to the optical phase retardation, which is the product of the birefringence Δn and the layer thickness t. The thickness of the liquid crystal layer in our devices is fixed to 5.5 µm by the addition of spherical spacers in the glue binding the two glass substrates together. The liquid crystal used in both devices is the nematic liquid crystal mixture E7 (Merck), which is uniaxially birefringent. The optical retardation is voltage dependent, because the liquid crystal director tends to align with the local electric field, if $\Delta\varepsilon > 0$. In the voltage-off state, the director is oriented along the direction imposed by the previously mentioned alignment layer.

To simplify the analysis, we use quasi-monochromatic light from a series of green LEDs ($\lambda_c = 520\,\text{nm}, \Delta\lambda_{\text{FWHM}} = 34\,\text{nm}$) rather than white light. For monochromatic light, transmission through a uniaxially birefringent material between two crossed polarizers is given by:

$$T = \sin^2(2\phi)\sin^2\left(\frac{\Gamma}{2}\right) \tag{2}$$

with ϕ the angle between the transmission axis of either of the polarizers and the projection of the director on the plane perpendicular to the light propagation direction, and Γ the retardation given by: $\Gamma = \frac{2\pi}{\lambda}\Delta n d$. Here, λ is the wavelength of light in vacuum, d is the thickness of the birefringent material and Δn is the birefringence. Equation 2 relates intensity differences to a medium's phase retardation. For a liquid crystal in vertical field switching mode, which is the case for our devices, the retardation is a function of the tilt of the director, which is in turn a function of the local electric field.

We took images with a digital camera mounted on top of the polarizing optical microscope while applying a voltage between the common and the ring-shaped electrodes. The latter were all kept at the same potential. Figure 3 shows the polarizing optical transmission microscope images of the reference device (left) and PZT-enhanced device (right). The dark concentric lines are the electrodes that are spaced 60 µm apart. These images were taken when a 1 kHz square wave was applied to the device, with a potential difference of 2 V between the ring-shaped electrodes and the common electrode. In the picture of the reference device, one can clearly see a large intensity variation close to the electrode edges. This is due to the reorientation of the liquid crystal director that aligns along the electric field lines. This reorientation leads to a change in the polarization of transmitted light, which results in a change in the amount of light that passes through the analyzer. In the PZT-enhanced device the region where the director reorients is much wider, indicating that the PZT layer has spread the electric potential further away from the electrodes. How far it spreads the electric field can be estimated from the intensity variations halfway between two neighboring electrodes: for the reference device no intensity variation is discernible there, but the PZT-enhanced lens shows a small decrease in intensity, which is apparent from the small overlay in the lower right corner. The addition of the PZT-layer increases the voltage drop across the LC halfway between two neighboring

#258864 Received 3 Feb 2016; revised 23 Mar 2016; accepted 27 Mar 2016; published 6 Apr 2016

electrodes, making it larger than the threshold voltage so that the liquid crystal starts to reorient.

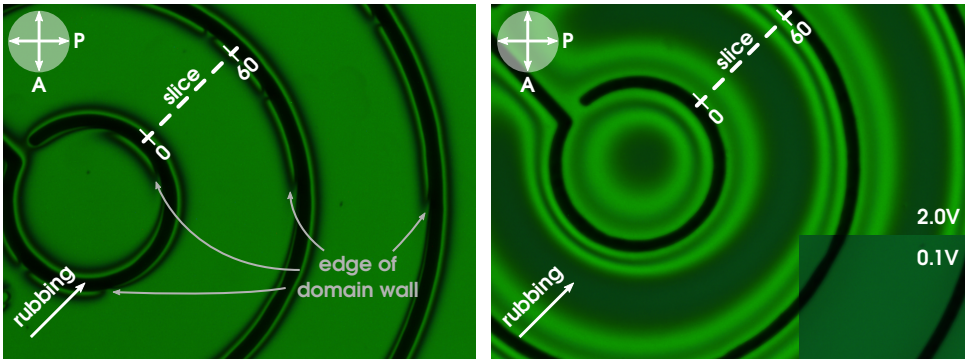

(a) Reference device (b) PZT-enhanced device

Fig. 3. Microscope images of a reference device (left) and a device with electrodes covered by 0.84 µm PZT (right), where the device is between crossed polarizers. The electrodes are 6 µm wide and spaced 60 µm apart; a 1 kHz square wave is connected to the electrodes, forming a potential difference of 2.0 V between the circular electrodes and the common electrode. The bottom right corner of the PZT-enhanced device shows the situation for the same lens when the amplitude is 0.1 V.

Interesting to note is that in the reference device domain walls are apparent, which collapse into disclination lines at higher voltages (∼7.8 V, see Visualization 1). The reason for their appearance is the presence of strong in-plane fringe fields which tilt the LC in a direction opposite to the one imposed by the pretilt [23], as shown by the simulation result of Fig. 4(a), which is a visualization of the director profile along the slice indicated in Fig. 3(a). [24] No domain walls are visible in the PZT-enhanced device [Fig. 3(b)], which demonstrates the ability to reduce fringe fields near electrode edges.

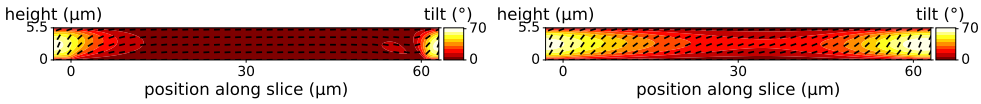

(a) Simulated slice through reference device (b) Simulated slice through enhanced device

Fig. 4. Cross-sections of the simulated director profile corresponding to the microscope images in Fig. 3. The position of these cross-sectional slices in the microscope images is indicated by a white dashed line. The addressing electrodes are not shown, but are located at the edges of the slice at a height of 0 µm in the reference lens and at −0.84 µm in the enhanced device.

A study of the radial intensity profile as a function of the applied voltage of the devices with 60 µm large inter-electrode distance was performed. The resulting imageset is available in the form of a movie from the publisher (Visualization 1). The information contained therein is summarized in Fig. 5: it shows the intensity profile along the rubbing direction between two consecutive electrodes for images that were taken with differing electric potentials applied between the common and the addressing electrodes. These graphs show the LC switching upon applying an electric field: each horizontal line corresponds to the intensity profile at a specific voltage at which the picture was taken. This "voltage-lapse" shows that the threshold voltage near the electrodes is hardly affected by the thin layer of PZT, but that the switching of the director is spreading further into the inter-electrode region, compared to the reference device. For a device with an inter-electrode distance of 30 µm, the intensity profile along the rubbing

#258864 Received 3 Feb 2016; revised 23 Mar 2016; accepted 27 Mar 2016; published 6 Apr 2016

direction for the PZT-enhanced device was nearly uniform. Figure 5 illustrates that the ability of the PZT layer to "smear" the electric field laterally between two electrodes to obtain a quasi-homogeneous electric field distribution over the LC layer is limited. This limitation can be overcome by increasing the thickness of the PZT layer, by further increasing its dielectric constant, by decreasing the permittivity of the liquid crystal or by increasing the liquid crystal layer thickness.

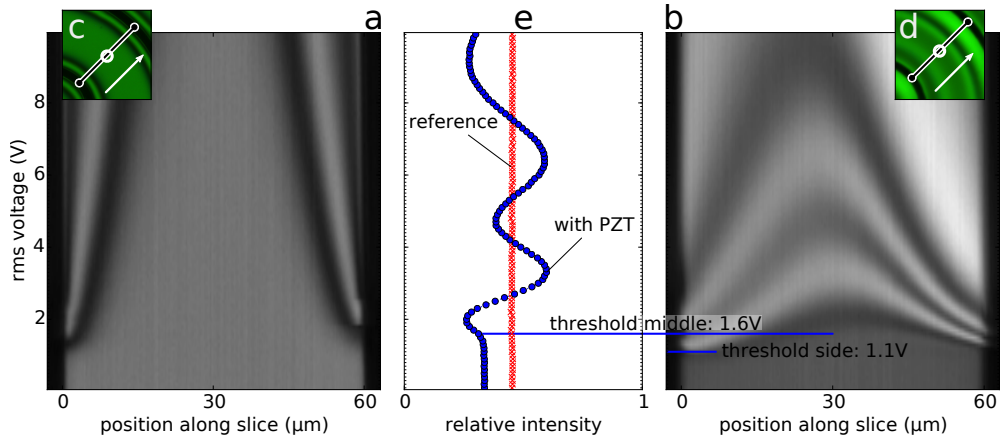

Fig. 5. The intensity profile maps, (a) and (b), show the relative transmission of the device between crossed polarizers as a function of the potential difference between the circular electrodes and the common electrode. (a) corresponds to the reference lens, (b) to the PZT-enhanced lens. The insets, (c) and (d), show the position along which the intensity profile is taken and the rubbing direction (see Visualization 1 for an overview of the intensity changes along different directions). These inset pictures reflect the situation at 5.1 V. The graph in (e) shows the intensity profiles halfway between the two electrodes. The oscillations in the intensity profile when a PZT layer is present (red dotted line) show that the liquid crystal director at 30 μm from the electrodes reorients at much lower voltages than those that would be required had the PZT layer not been present.

With the effect of the PZT layer on the distribution of the electric field being demonstrated, we tested the focusing ability of the PZT-enhanced liquid crystal lens with 30 μm inter-electrode spacing. By applying well-chosen electric potentials to the addressing electrodes, it is possible to obtain a nearly parabolic phase profile. The lens design with eight electrodes can focus a beam of light at different focal lengths, depending on the set of voltages applied. The strongest focusing power can be realized by choosing the voltages in such a way that at the outer electrode the liquid crystal director is fully tilted, so that light experiences the ordinary refractive index. The voltage decreases in a non-linear way towards the electrode at the center, where a voltage just below threshold is over the liquid crystal so that the polarized light experiences the extraordinary refractive index. In this way, a lens with focal length of $f \approx r^2/(2\Delta n d)$ is obtained, where r is the radius of the lens, Δn the index difference experienced by light at the edge and the center and d the thickness of the LC layer [25]. For the lens considered in this work, this means that the tuning range of the focal distance is from infinity (no focusing) to 3.4 cm.

We have focused an expanded laser beam ($\lambda_{\mathrm{HeNe}} = 632.8\,\mathrm{nm}$), linearly polarized along the rubbing direction of the LC lens, based on a "strong" and a "weak" retardation profile, which results in the beam being focused at a distance of 4.4 cm and 7.4 cm respectively. Figure 6(a) shows a close-up of the lens taken with a 10X microscope objective when all electrodes were grounded. The contours of the metallic electrodes are visible, and there are some intensity vari-

#258864 Received 3 Feb 2016; revised 23 Mar 2016; accepted 27 Mar 2016; published 6 Apr 2016

ations related to inhomogeneities in the incoming beam and the imaging system. At a distance of 4.4 cm the OFF-pattern is that of Fig. 6(b). A dark disc in the center, smaller than the actual lens, is distinguishable; it originates from the shadows of the circular electrodes. When the appropriate set of voltages is applied to the electrodes, we obtain an intense, small spot [Fig. 6(e)], surrounded by a region that is 21 times darker and about the size of the actual lens, as shown by the radial intensity profile in Fig. 6(d). This indicates that most of the light passing through the lens aperture is focused to the center. Similar conclusions can be drawn from Fig. 6(c) and Fig. 6(f), where the experiment was repeated, but with focal distance of the tunable lens equal to 7.4 cm.

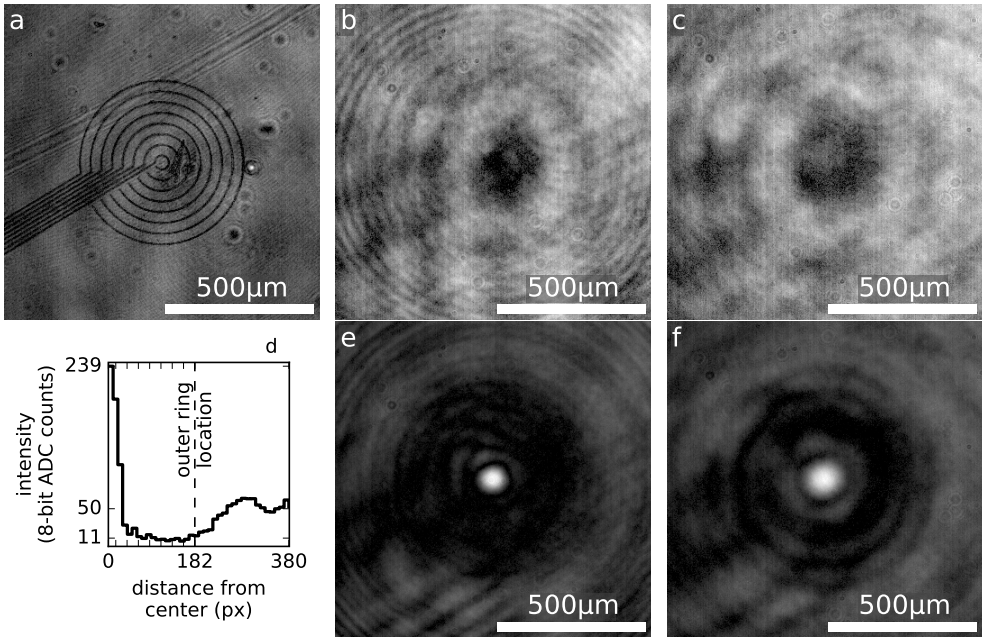

Fig. 6. Image set of a PZT-enhanced lens with 30 µm inter-electrode spacing. These images were taken with a 10X microscope objective in front of the camera sensor. (a) Transmission image of the microlens illuminated by the laser when no voltages are applied. The image plane of pictures (b), (e) and (c), (f) is 4.4 cm and 7.4 cm away from the lens electrode plane respectively. The upper row shows the intensity distribution when no potential is applied to the lens electrodes, whereas in the bottom row an appropriate set of voltages was applied to obtain a small, intense focused spot. The graph (d) shows the radial intensity profile of the focused spot of subfigure (e).

These pictures indicate that most of the light is redirected to the focal spot, which means that there is indeed a smooth director variation between the 30 µm spaced electrodes. This gradual variation is made possible by the presence of the PZT layer. The aberrations are due to the use of non-transparent metallic electrodes. This could be overcome by using a transparent conductor such as ITO.

We compare the spot profile shown in Fig. 6(e) to that of a similar-sized and diffraction-limited lens. An ideal lens will focus a laser beam down to a spot known as the Airy disc, which together with the lower-intensity concentric rings around it form the Airy pattern. The full width at half maximum (FWHM) of this diffraction limited spot is given by $D_{\mathrm{FWHM}} = 1.02\lambda\frac{f}{d}$ with D the diameter of this region, f the focal length of the lens and d the diameter of the focusing lens. For an ideal lens with focal length of $f = 4.4$ cm and a diameter of $d = 557$ µm, this would result in a FWHM of the Airy disc of 51 µm. The diameter in this situation is chosen to be

#258864 Received 3 Feb 2016; revised 23 Mar 2016; accepted 27 Mar 2016; published 6 Apr 2016

equal to the largest outer diameter of the set of concentric ring-shaped electrodes of the liquid crystal lens. In reality a small region around the electrodes still contributes towards the lensing operation, so the chosen diameter is slightly underestimated. The FWHM of the focused spot, shown in Fig. 6(e) is measured to be 72 µm, about 41 % larger than that of the theoretical ideal.

4. Conclusion

We have demonstrated that a 0.84 µm thick PZT layer with a high dielectric constant can be used to induce a smoothly varying phase profile in liquid-crystal-based beam-steering devices. Because PZT is optically transparent, it can be used to reduce the area that is covered by electrodes, and avoid the use of ITO. The parameters that determine the maximum possible electrode spacing are the dielectric constant of the layer, its thickness and the dielectric constant and thickness of the liquid crystal layer on top of it. Furthermore, because PZT is a dielectric, no additional current flows through the device, resulting in applications that consume little power, a desirable property for e.g. handheld devices. The combination of a grid of metallic electrodes with a PZT layer could also be used as a uniform transparent conductor, i.e. a replacement for ITO.

Acknowledgments

The authors acknowledge financial support from the "Agentschap voor Innovatie door Wetenschap en Technologie" IWT through the SBO project SECONDOS, IWT-nr 120019, 2013-2016, as well as the Interuniversity Attraction Poles program of the Belgian Science Policy Office, under grant IAP P7-35 (Photonics@be). We wish to thank Steven Verstuyft, from Ghent University, INTEC/Photonics, for his supervision and critical eye during the image reversal step of the lithography and David Schenk (IDnA) for creating a schematic render of the lens device.

#258864 Received 3 Feb 2016; revised 23 Mar 2016; accepted 27 Mar 2016; published 6 Apr 2016